PNAS RESEARCH ARTICLE | IMMUNOLOGY AND INFLAMMATION

Cytosolic proliferating cell nuclear antigen (PCNA) orchestrates neutrophil hyperactivation in COVID-19

Rodrigo de Oliveira Formiga[a,b,c], Lucie Pesenti[a,b], François Chable de la Héronnière[a,b], Maha Zohra Ladjemi[a,b], Darko Stojkov[d], Shida Yousefi[d], Philippe Frachet[e], Lisa Krafft[f], Laura Tiberio[g], Daniela Bosisio[g], Muriel Andrieu[a,b], Souganya Many[a,b], Vaarany Karunanithy[a,b], Karine Bailly[a,b], Théo Dhôte[a,b], Giovanni Saraceni-Tasso[a,b], Manon Castel[a,b], Christophe Rousseau[a,b], Marick Rodrigues Starick[c], Edroaldo Lummertz da Rocha[h], Emilia Puig Lombardi[i], Cicero José Luíz dos Ramos Almeida[j], Anderson dos Santos Ramos[j], Fernando Queiroz Cunha[j], José Carlos Alves-Filho[j], Natália Ribeiro Cabacinha Nóbrega[k], Matheus Rodrigues Gonçalves[l], Celso Martins Queiroz-Junior[k], Viviane Lima Batista[l], Mauro Martins Teixeira[m], Vanessa Granger[n,o], Sylvie Chollet-Martin[n,o], Luc De Chaisemartin[n,o], Luc Mouthon[a,p], Anne Hosmalin[a,b], Margarita Hurtado-Nedelec[q], Clémence Martin[a,b,r], Fernando Spiller[c], Hans-Uwe Simon[d,s], Nicolas Tamassia[t], Marco Antonio Cassatella[t], Frédéric Pène[a,b,u], Thomas Vogl[f], Pierre-Regis Burgel[a,b,r], Vivian Vasconcelos Costa[k], and Véronique Witko-Sarsat[a,b,1]

Affiliations are included on p. 12.

Edited by Carl Nathan, Weill Cornell Medicine, New York, NY; received February 19, 2025; accepted September 12, 2025

Neutrophils are central mediators of the hyperinflammatory response in severe SARS-CoV-2 infection. We report elevated cytosolic levels of proliferating cell nuclear antigen (PCNA) in neutrophils from patients with severe and critical COVID-19, correlating with enhanced NADPH oxidase–dependent reactive oxygen species (ROS) generation and neutrophil extracellular trap (NET) formation. Using T2AA, a small-molecule inhibitor of the PCNA scaffold, we demonstrate potent suppression of NADPH oxidase activation and NET release, particularly in response to SARS-CoV-2 RNA. Mechanistically, we identify a previously unrecognized interaction between PCNA and the heterodimeric S100A8/S100A9 (calprotectin), predominantly enriched in $CD16^{high}CD62L^{low}$ neutrophils expanded during COVID-19. PCNA binds the dimeric S100A8/S100A9 complex mediated via S100A8 subunit with micromolar affinity, and this interaction is abrogated by tetramerization, suggesting regulation by intracellular calcium. Disruption of this complex by T2AA inhibited ROS production in an S100A8/S100A9-dependent manner, implicating calprotectin as a functional regulator of neutrophil activation. In a betacoronavirus mouse model, T2AA treatment attenuated lung inflammation, reduced NET and calprotectin levels, and shifted pulmonary neutrophils away from hyperactivated and immunosuppressive phenotypes, consistent with immune reprogramming toward resolution. These findings establish cytosolic PCNA as a central scaffold in neutrophil hyperactivation during COVID-19 and highlight its pharmacological disruption as a promising host-directed strategy to limit inflammation and prevent organ damage.

neutrophils | COVID-19 | PCNA

Significance

Severe COVID-19 is marked by excessive neutrophil activation, leading to the release of damaging molecules that injure the lungs and other organs. While neutrophil hyperactivation is a hallmark of severe disease, the molecular mechanisms that sustain this response are not fully characterized. Here, we identify cytosolic PCNA as a central organizer of neutrophil responses through its interaction with the inflammatory protein calprotectin. Disrupting this interaction with the small molecule T2AA attenuates neutrophil-driven inflammation, highlighting a potential therapeutic strategy to limit tissue damage in severe SARS-CoV-2 infection.

Neutrophils are key players in the innate immune response and form the first line of defense against infectious agents, as they employ well-characterized antimicrobial strategies, such as the release of reactive oxygen species (ROS), neutrophil extracellular traps (NETs), and other proinflammatory mediators (1). Recent unexpected biological features related to their phenotypic and functional heterogeneity (2–5) have been highlighted in Coronavirus Disease (COVID)-19 caused by the severe acute respiratory syndrome coronavirus 2 (SARS-CoV-2) (6), such as increased counts and newly identified subsets with aberrant characteristics in both circulation and infiltrated into the respiratory tract (2, 3, 7–9). Upon SARS-CoV-2 infection, a wide spectrum of clinical outcomes may appear, ranging from self-limited asymptomatic (10) or mild disease to severe cases, the last marked by thromboembolic events, dysregulated immune response, respiratory distress, and multiorgan failure (3, 4, 9, 11, 12).

Neutrophil-derived mediators, such as the S100A8/S100A9 heterodimer, also known as calprotectin (13), and NETs composed of extracellular DNA bound to granule-derived proteases (14), are found at high levels in sera from COVID-19 patients and are strongly associated with disease severity and poor prognosis (7, 15). Calprotectin is a key regulator of neutrophil activation, promoting cytoskeletal rearrangement, arachidonic acid metabolism, and NADPH-oxidase complex assembly (13) and is also associated with NET (16).

In COVID-19, NET formation depends in part on ROS production, but also on the direct interaction with single-strand RNA from the SARS-CoV-2 genome via a

This article is a PNAS Direct Submission.

[1]To whom correspondence may be addressed. Email: veronique.witko@inserm.fr.

This article contains supporting information online at https://www.pnas.org/lookup/suppl/doi:10.1073/pnas.2503667122/-/DCSupplemental.

Published October 21, 2025.

TLR-8-dependent mechanism (17), contributing to neutrophil hyperactivation and tissue damage (12).

To understand neutrophil dysregulation in COVID-19, we examined the proliferating cell nuclear antigen (PCNA), previously described by our group as a key regulator of neutrophil fate (18–20). While PCNA contributes to DNA replication and repair in proliferating cells (21), in neutrophils, it is exclusively cytoplasmic, promoting cell survival through interactions with procaspases (18, 22) and ROS-production via direct binding to NADPH-oxidase components (19, 20). PCNA scaffold is highly influenced by the inflammatory environment. In granulocyte-colony stimulating factor (G-CSF) treated donors PCNA interactome is reshaped to coordinate cellular functions via glycolytic-associated metabolic reprogramming (20). Recently, we provide evidence of profound changes in the overall PCNA scaffold in neutrophils from COVID-19 patients with a strong interferon signature (23). Pertinently, PCNA-dependent functions may be targeted using the small molecule T2 amino alcohol (T2AA) (24), which has shown beneficial properties against gut inflammation by regulating neutrophil ROS production (19).

Therefore, we here sought to determine whether and how PCNA contributes to this intricate interplay driving neutrophil dysregulation in COVID-19. We identify an activation axis in which cytosolic PCNA scaffold regulates NADPH-oxidase driven ROS production, influencing NET formation in hyperactivated neutrophils of severe COVID-19 patients. Notably, we describe the association between PCNA and S100A8/S100A9 heterodimer that was promoted in a distinct subset of activated neutrophil in COVID-19 patients. We also show that targeting the PCNA-dependent mechanism in a murine model of COVID-19-like lung inflammation could constitute a valuable strategy to mitigate excessive inflammation in severe COVID-19 and other inflammatory diseases.

Results

Increased PCNA Expression in Neutrophils Is Associated With COVID-19 Severity and Increased Cell Survival and NADPH-Oxidase-Dependent ROS. Western blot analysis of neutrophils from healthy donors (HD) and COVID-19 patients showed a significant increase in cytosolic PCNA expression, correlating with disease severity. Severe and critical patients, but not mild cases, had higher PCNA levels than HD (Fig. 1 *A* and *B* and *SI Appendix*, Table S1). Immunofluorescence confirmed PCNA's exclusive cytoplasmic localization (Fig. 1 *C* and *D*). Notably, scRNA-seq reanalysis (7, 25) showed no significant changes in PCNA mRNA in circulating or respiratory tract neutrophils from severe COVID-19 patients (*SI Appendix*, Figs. S1 and S2), suggesting posttranscriptional stabilization, consistent with prior findings in inflammation (18). Next, we assessed neutrophil viability after 16 h in vitro. Severe and critical COVID-19 neutrophils exhibited higher survival (Annexin-V^-/7-AAD^-) and reduced apoptosis (Annexin-V^+/7-AAD^-) and necrosis (Annexin-V^+/7-AAD^+) (Fig. 1 *E*–*G*). DiOC6 staining confirmed better-preserved mitochondrial membrane potential ($\Delta\psi m$) (Fig. 1*H*). Notably, PCNA inhibition with T2AA disrupted the scaffold, significantly affecting apoptosis and $\Delta\psi m$ in COVID-19 neutrophils without changing necrosis (Fig. 1 *E*–*H*). Such results underscore PCNA's role in sustaining survival and its potential impact on the resolution of inflammation.

To assess the implication of PCNA on neutrophil activation in COVID-19, we measured NADPH-oxidase-dependent ROS production. Neutrophils from severe and critical patients showed significantly higher basal and phorbol 12-myristate 13-acetate (PMA)-induced ROS levels, unlike those from mild cases. T2AA inhibition of the PCNA scaffold reduced both basal and stimulated ROS production across all severities (Fig. 1 *I* and *J*). Enhanced ROS production was also triggered by N-formylmethionyl-leucyl-phenylalanine (fMLF) or opsonized zymosan, indicating a primed neutrophil state independent of specific NADPH-oxidase activation pathways. Notably, T2AA was more effective in reducing ROS in COVID-19 neutrophils than in HD (*SI Appendix*, Fig. S3).

Elevated PCNA Expression Is Associated With NET Formation in COVID-19 Neutrophils. Given the role of NET formation in COVID-19 pathology, we examined its link to cytosolic PCNA and ROS. Circulating NETs were elevated in COVID-19 patients (Fig. 2*A*) and positively correlated with ROS production (Fig. 2*B*) and cytosolic PCNA (Fig. 2*C*). To test PCNA's role in NET formation, HD neutrophils were stimulated for 35 min with granulocyte-macrophage colony-stimulating factor (GM-CSF) and C5a, factors elevated in severe COVID-19 (26, 27), to induce NETs without triggering death (28). On the other hand, PMA at different time points (20 min, 1 h, 2 h) was used to induce nuclear and mitochondrial DNA release (29). Both T2AA and DPI, a selective NADPH-oxidase inhibitor (30), significantly reduced NET release induced by GM-CSF/C5a and PMA at early time points (Fig. 2 *D* and *E*), suggesting that T2AA controls ROS production and NET release via NADPH-oxidase inhibition. We next evaluated whether T2AA could modulate NET formation induced by single-stranded RNA from the SARS-CoV-2 genome (ssRNA) (17). As shown in Fig. 2*F*, stimulation of neutrophils from HD with ssRNA led to a significant increase in DNA-associated elastase activity, indicative of NET release. Pretreatment with T2AA reduced elastase activity in a dose-dependent manner, with significant inhibition observed at 10 and 20 μM. A similar inhibitory effect was seen with CU-CPT9a, a selective inhibitor of Toll-like receptor 8 (TLR8) used here as a positive control to inhibit viral RNA-induced NET formation. Consistent with these results, immunofluorescence imaging revealed extensive NET structures marked by citrullinated histone H4 (Cit-H4) following ssRNA stimulation, which were markedly diminished in neutrophils treated with either T2AA or CU-CPT9a (Fig. 2*G*). These findings suggest that cytosolic PCNA contributes to NET formation particularly in response to viral RNA, and that T2AA, by effectively interfering with this process, might have potential therapeutic value in COVID-19.

S100A8 Is a Partner of PCNA Which Is Overexpressed in Neutrophils from COVID-19 Patients. Since S100A8/S100A9 is linked to neutrophil activation and COVID-19 severity (7), we investigated its potential involvement in PCNA-induced neutrophil dysregulation. Western blot analysis revealed high S100A8 expression in neutrophil cytosols from severe and critical cases (Fig. 3 *A* and *B*), a finding supported by immunofluorescence showing stronger cytosolic staining in these patients (*SI Appendix*, Fig. S4 *A* and *B*). Serum calprotectin levels were also elevated in a severity-dependent manner (*SI Appendix*, Fig. S4*C*). Unlike PCNA, scRNA-seq data showed increased S100A8 and S100A9 mRNA in peripheral neutrophils, with higher S100A8 in respiratory tract-infiltrating neutrophils, particularly in critical cases (*SI Appendix*, Figs. S1 and S2). Calprotectin cytosolic levels correlated with cytosolic PCNA (Fig. 3*C*). Additionally, circulating neutrophil elastase amounts were also elevated in severe/critical COVID-19 and correlated with serum calprotectin, PCNA, and NETs (*SI Appendix*, Fig. S4 *D*–*G*).

To assess whether S100A8/S100A9 could directly interact with PCNA, we performed a proximity ligation assay (PLA). The results

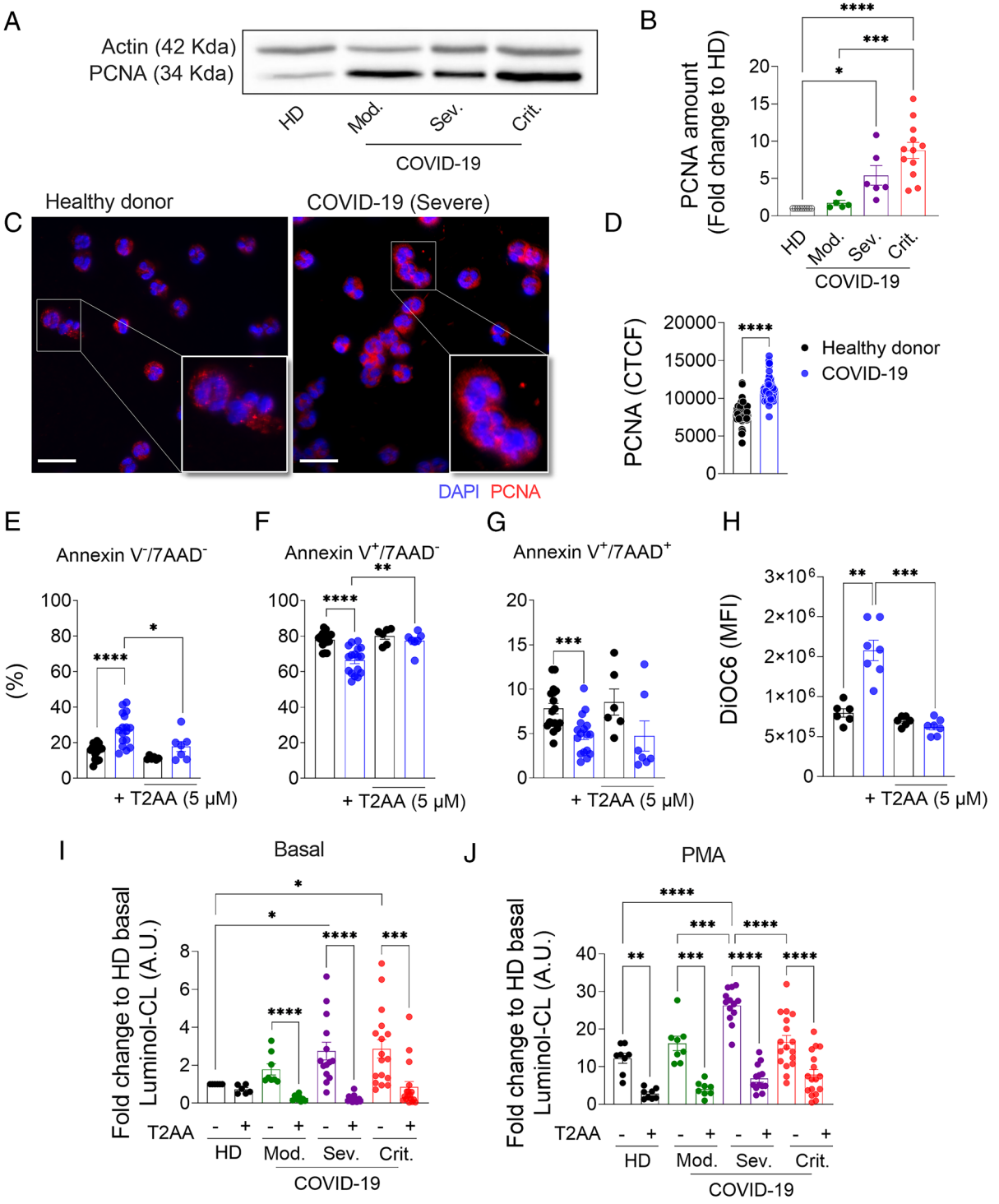

Fig. 1. PCNA is overexpressed in neutrophil cytosol according to COVID-19 severity and linked to increased survival and NADPH-oxidase-dependent ROS production. (*A* and *B*) Western blot of PCNA in neutrophil cytosols from HD (n = 9), moderate (n = 5), severe (n = 6), and critical (n = 12) COVID-19 patients. (*A*) Representative blot. (*B*) Densitometry (fold change vs HD). Mean ± SEM; analyzed by one-way ANOVA followed by the Tukey post test (*$P < 0.05$, ***$P < 0.001$, ****$P < 0.0001$). (*C* and *D*) Immunofluorescence of neutrophils from HD (n = 5) and severe/critical patients (n = 5) stained for PCNA (red) and nuclei (DAPI, blue). (*C*) Representative images. (Scale bar, 20 μm.) (*D*) Corrected total cell fluorescence (CTCF) from n = 150 cells/group. Mean ± SEM; analyzed by Mann–Whitney *U* test (****$P < 0.0001$). (*E*–*H*) Neutrophils incubated for 16 h at 37 °C, 5% CO_2. Percentages of viable (*E*), apoptotic (*F*), and necrotic (*G*) cells from HD (n = 17, with or without T2AA 5 μM, n = 6) and severe/critical patients (n = 17, with or without T2AA, n = 7). (*H*) DiOC6 MFI (mitochondrial membrane integrity) in HD (n = 6) and severe/critical patients (n = 7). Mean ± SEM; analyzed by the unpaired *t* test (*$P < 0.05$, **$P < 0.01$, ***$P < 0.001$, ****$P < 0.0001$). (*I* and *J*) ROS production via luminol-enhanced chemiluminescence (CL) with or without T2AA (5 μM) at 37 °C. (*I*) Basal neutrophils from HD (n = 6), moderate (n = 8), severe (n = 14), and critical (n = 17). (*J*) PMA-stimulated neutrophils from HD (n = 8), moderate (n = 8), severe (n = 13), and critical (n = 17). Data are expressed as arbitrary units (A.U.) fold change to unstimulated HD at ROS peak, mean ± SEM; analyzed by the unpaired *t* test (untreated vs COVID-19) or paired *t* test (with vs without T2AA) (*$P < 0.05$, **$P < 0.01$, ***$P < 0.001$, ****$P < 0.0001$).

revealed cytoplasmic interactions between PCNA and both S100A8 (Fig. 3 *D* and *E*) and S100A9 (Fig. 3*F*) in neutrophils from HD, with significantly stronger PLA signals observed in neutrophils from patients with severe COVID-19, suggesting an association with both subunits of calprotectin, the predominant cytosolic form in neutrophils (13). Notably, treatment with T2AA,

Table 1. Kinetics and affinity of PCNA interaction with S100A8 and S100A8-S100A9N69A

	PCNA/S100A8		PCNA/S100A8-S100A9N69A
Immobilized ligand/Soluble analyte	Heterogenous ligand model	1:1 model	1:1 model
K_{a1} (M^{-1} s^{-1})	2,199	158.5	4,087
K_{d1} (s^{-1})	0.1035	0.00568	0.001854
K_{a2} (M^{-1} s^{-1})	138.1	NA	NA
K_{d2} (s^{-1})	0.0034	NA	NA
KD (M)	4.7×10^{-5} (*KD1*) 2.49×10^{-5} (*KD2*)	3.58×10^{-5}	4.54×10^{-7}
Chi^2	7.6	16.6	8

Binding of S100A8 (0.1 to 2 μM) and S100A8-S100A9N69A (0.062 to 0.5 μM) was assessed as described in *Materials and Methods*. Data were fitted using 1:1 or heterogeneous ligand models when provided a better Chi^2 value. The heterogeneous ligand model accounts for two different binding sites on the immobilized PCNA, yielding KD1 and KD2 were determined. NA = not applicable.

which disrupts PCNA's cytosolic scaffold function, markedly reduced the PCNA–S100A8 interaction, an effect particularly pronounced in COVID-19 neutrophils (Fig. 3 *D* and *E*). Furthermore, surface plasmon resonance (SPR) also demonstrated that S100A8 bound directly to immobilized PCNA with a micromolar affinity (KD = 35 μM). S100A9 alone did not bind, and the wild-type S100A8/S100A9 heterodimer also failed to bind PCNA in our biophysical setting (Fig. 3*G* and Table 1 and *SI Appendix*, Fig. S5), likely due to its ability to form tetramers in the presence of calcium (31). In contrast, the S100A8–S100A9 N69A mutant complex, which is deficient in tetramerization, showed specific, dose-dependent binding to immobilized PCNA with a better affinity and a lower KD than those observed for S100A8 (KD = 0.454 μM) (Fig. 3*H* and Table 1). Altogether, this is indicative that S100A8 mediates the interaction between the heterodimer and PCNA thereby suggesting a potential regulatory role of PCNA on calprotectin biological activities.

To further clarify the functional role of the PCNA–S100A8/S100A9 interaction, we investigated whether this association is modulated by NADPH oxidase activity, given that both PCNA and S100A8/S100A9 contribute to its regulation (19, 32, 33). In neutrophils, PLA analysis revealed that PCNA–S100A8 association is increased following fMLF-induced NADPH oxidase activation and decreased upon T2AA treatment (Fig. 4 *A* and *B*). Conversely, to test whether NADPH oxidase activity could affect PCNA–S100A8 association, we examined the effect of T2AA in wild type (WT) or $gp91^{phox}$ knock out (KO) neutrophil-like PLB-985 cells, which lack NADPH-dependent ROS production (Fig. 4 *C*–*G*). Cells differentiated with *N*,*N*-dimethylformamide (DMF) acquire a neutrophil-like phenotype expressing higher CD11b membrane levels. WT and KO cells showed similar amounts of CD11b confirming efficient differentiation in the two settings (Fig. 4*C*). Besides, consistent with our observations in neutrophils, T2AA inhibited NADPH oxidase–derived ROS in WT cells under various stimuli, whereas $gp91^{phox}$ KO cells produced no detectable ROS (Fig. 4 *D* and *E*). Similarly, PLA showed that PCNA–S100A8 interactions were present at resting and further elevated after fMLF stimulation in wild-type PLB-985 cells (Fig. 4 *F* and *G*). In contrast, although $gp91^{phox}$ KO cells exhibited detectable PCNA–S100A8 association at baseline, fMLF stimulation failed to induce the increase observed in WT cells. This suggests that NADPH oxidase assembly is necessary to sustain or enhance PCNA–S100A8 binding upon activation. Finally, using differentiated HoxB8 cells allowing the analysis of neutrophil functions after specific genetic editing (34), we analyzed HoxB8 S100A9-KO cells, which are also deficient in S100A8/S100A9 (35). In these cells, T2AA failed to inhibit the PMA-induced respiratory burst, whereas WT cells showed significant reduction in ROS production under the same conditions (Fig. 4 *H* and *I*). Together, these data suggest that the PCNA–S100A8/S100A9 association has a functional role upon activation and is both a regulator and a target of NADPH oxidase activity.

PCNA-S100A8 Cytosolic Interaction Is Increased in a Hyperactivated Subset of $CD16^{high}/CD62L^{low}$ Neutrophils in Severe and Critical COVID-19. Owing to the neutrophil heterogeneity in COVID-19, we investigated whether the PCNA-S100A8 interaction is linked to specific neutrophil subsets in severe and critical disease. Using a broad flow cytometry panel (*SI Appendix*, Fig. S6), we found that $CD15^{+}$ neutrophils from severe/critical patients exhibited increased markers (CD11b, CD45, CD66b, LOX-1, PDL-1, CD114) and decreased CD62L, indicating intense activation. Additionally, CD10 expression was reduced, suggesting immaturity, while CD16, CD15, PD-1, CD33, and GLUT-1 remained unchanged. Dysregulation of neutrophil immunophenotype was also observed in the low-density neutrophil (LDN) fraction (*SI Appendix*, Fig. S7). These findings support the emergence of an aberrant neutrophil subset in severe COVID-19.

To assess whether PCNA-S100A8 interaction marks neutrophil heterogeneity, we analyzed CD16/CD62L markers (36) also reported to differentiate distinct neutrophil subsets in COVID-19 (37, 38). In HD, most neutrophils were conventional $CD16^{high}/CD62L^{high}$, while other subsets ($CD16^{high}/CD62L^{low}$, $CD16^{low}/CD62L^{low}$, $CD16^{low}/CD62L^{high}$) each accounted for <1%. In contrast, severe/critical COVID-19 patients showed expansion of these alternative subsets with a reduction in conventional neutrophils (Fig. 5 *A* and *B*). PLA combined with CD16/CD62L immunolabeling revealed that in HD, PCNA-S100A8 interaction was highest in the conventional subset, whereas in COVID-19, it shifted to the hyperactivated $CD16^{high}/CD62L^{low}$ population (Fig. 5*C* and *SI Appendix*, Fig. S8).

ROS production analysis using the DCFCH staining showed that all neutrophil subsets in COVID-19 generated more ROS than their HD counterparts (Fig. 5*D*), both at baseline and upon PMA/opsonized zymosan stimulation (*SI Appendix*, Fig. S9). In HD, despite lower PCNA-S100A8 interaction, the $CD16^{high}/CD62L^{low}$ subset (≤3% of neutrophils) produced more ROS than the conventional one. However, in COVID-19, the highest ROS levels were observed in $CD16^{high}/CD62L^{low}$ neutrophils, which also exhibited the strongest PCNA-S100A8 interaction.

In COVID-19 patients, the $CD16^{high}/CD62L^{low}$ neutrophil subset showed the highest expression of CD11b (Fig. 5*E*) and LOX-1 (Fig. 5*F*) compared to the conventional subset. A

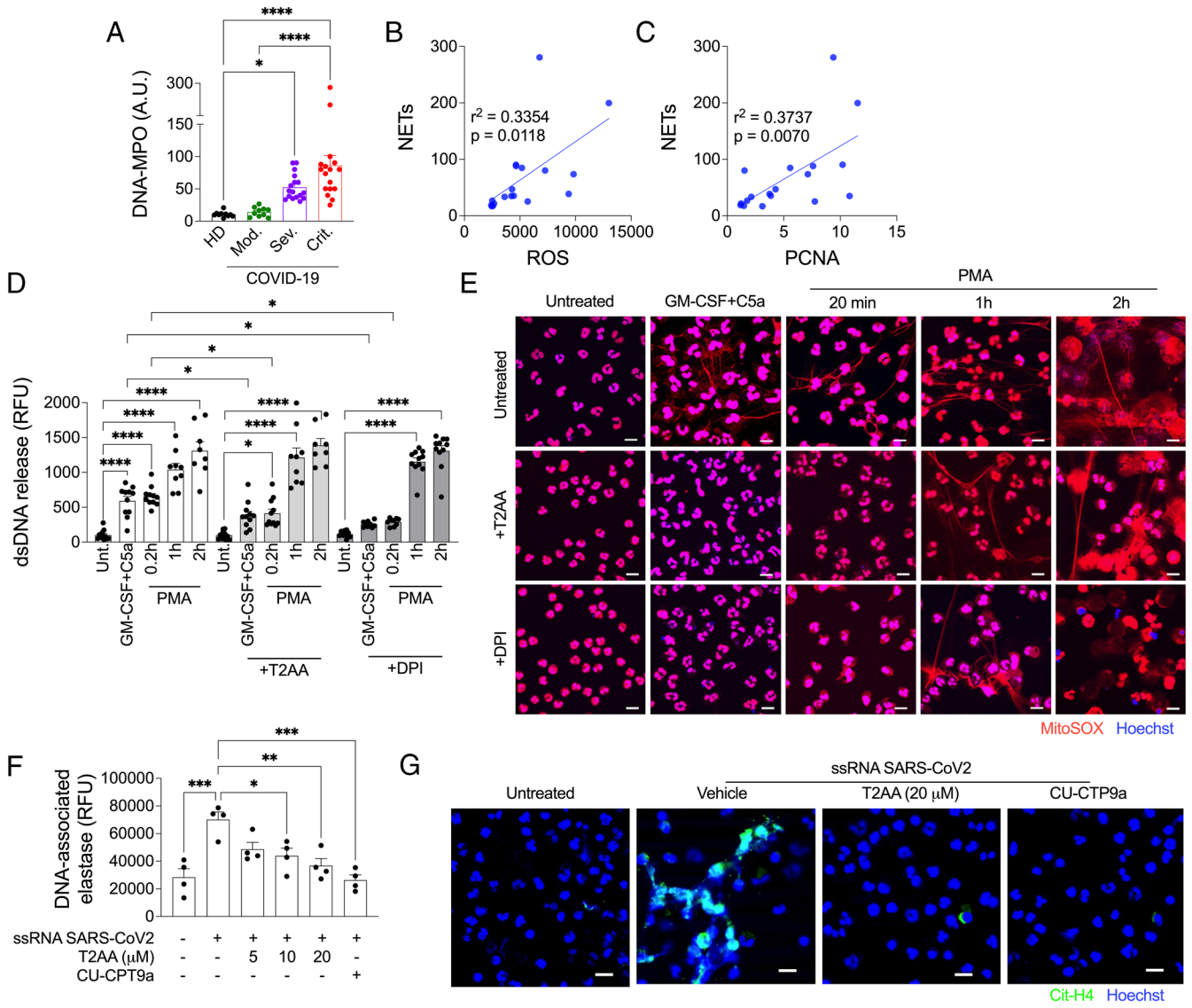

Fig. 2. PCNA is involved in NET formation in COVID-19. (*A*) NET levels measured as MPO–DNA complexes by ELISA in serum from HD (n = 10), moderate (n = 10), severe (n = 17), and critical (n = 17) COVID-19 patients. Mean ± SEM; analyzed by one-way ANOVA followed by the Tukey post test (*$P < 0.05$, ****$P < 0.0001$). (*B* and *C*) Correlations between NET levels and basal ROS production (*B*) or cytosolic PCNA expression (*C*). Pearson correlation: $P = 0.018$ (ROS), $P = 0.007$ (PCNA). (*D* and *E*) Neutrophils from HD (n = 8 to 12 per condition) preincubated with T2AA (10 μM), DPI (10 μM), or untreated for 30 min, then primed with GM-CSF plus C5a (35 min) or activated with PMA (20 min, 1 h, 2 h). (*D*) Quantification of released dsDNA in supernatants (n = 4 to 11) by PicoGreen assay. Mean ± SEM; analyzed by one-way ANOVA followed by the Tukey post test (*$P < 0.05$, ****$P < 0.0001$). (*E*) Representative confocal image of extracellular DNA (MitoSOX Red) and nuclei (Hoechst 33342). (Scale bar, 10 μm.) (*F* and *G*) Neutrophils from HD (n = 4) preincubated with T2AA (5, 10, or 20 μM), CU-CPT9a (20 μM), or untreated for 30 min, then stimulated or not with SARS-CoV-2 ssRNA for 4 h (*F*) or 1 h (*G*). (*F*) DNA-associated elastase in supernatants measured via elastase activity on fluorogenic substrate. Mean ± SEM; analyzed by one-way ANOVA followed by the Tukey post test (*$P < 0.05$, **$P < 0.01$, ***$P < 0.001$). (*G*) Representative NET images showing citrullinated histone-H4 (Cit-H4, green) and DNA (blue). (Scale bar, 10 μm.)

similar increase in CD11b was observed in HD, though at significantly lower levels. For LOX-1, no such difference was seen between subsets in HD, and overall expression was markedly lower than in COVID-19 neutrophils. CD10 expression (Fig. 5*G*) tended to be reduced in $CD16^{high}/CD62L^{low}$ cells from COVID-19 patients, with the lowest levels observed in the $CD16^{low}/CD62L^{low}$ subset, a pattern also seen in HD. However, in COVID-19, $CD16^{high}/CD62L^{low}$ neutrophils displayed significantly lower CD10 levels than other subsets. Collectively, these findings highlight the intense neutrophil reprogramming in severe and critical COVID-19 and present a strong link between PCNA-S100A8 interaction and elevated ROS production, particularly within a hyperactivated neutrophil subset.

Targeting PCNA Scaffold During a Betacoronavirus-Induced COVID-19-Like Lung Inflammation In Vivo Elicits Beneficial Effects Through the Regulation of Neutrophils Response. Intranasal infection of C57BL/6 mice with murine hepatitis virus strain 3 (MHV-3) is a well-established model for studying acute COVID-19 pathogenesis (Fig. 6*A*) (39) and testing novel therapies (5, 40, 41). Mice treated with T2AA showed no significant difference in viral titers compared to vehicle-treated mice (Fig. 6*B*), however, it reduced lung manifestations by lowering clinical scores (Fig. 6*C*), inflammatory injury, and improving lung tissue architecture (Fig. 6 *D* and *E*). T2AA also elevated total blood counts, partially improving lymphopenia and significantly increasing circulating granulocytes (Fig. 6*F*). To further assess the in vivo impact of T2AA, we analyzed pulmonary neutrophils

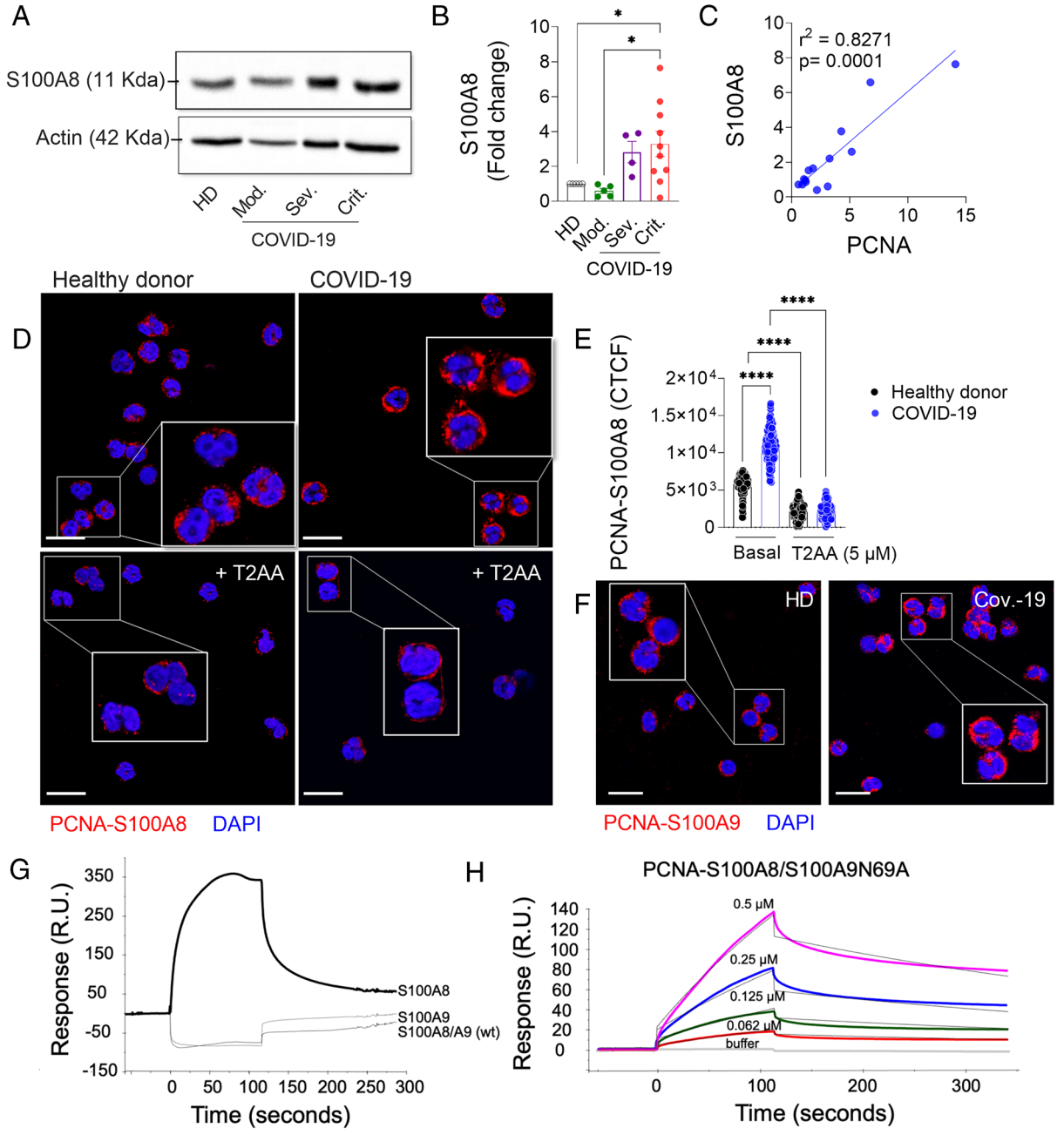

Fig. 3. S100A8 is overexpressed in neutrophil cytosols from COVID-19 patients and interacts with PCNA. (*A* and *B*) Western blot analysis of S100A8 in neutrophil cytosols from HD (n = 5), moderate (n = 5), severe (n = 4), and critical (n = 10) COVID-19 patients. (*A*) Representative blot. (*B*) Densitometry normalized to actin. Mean ± SEM; analyzed by one-way ANOVA followed by the Tukey post test (*$P < 0.05$). (*C*) Correlation between PCNA and calprotectin cytosolic levels in neutrophils by Western blot ($P = 0.0001$). (*D–F*) Duolink® proximity ligation assay (PLA) detecting PCNA–S100A8 (*D*) or PCNA–S100A9 (*F*) interactions in neutrophils (n = 5 per group). Fluorescence in red indicates protein proximity; nuclei in blue. (*D* and *E*) PLA showing effect of T2AA (5 μM, 30 min) on PCNA–S100A8 interaction. (*E*) PCNA–S100A8 signal as CTCF for n = 150 cells/group. Mean ± SEM; analyzed by Mann–Whitney *U* test (****$P < 0.0001$). (Scale bar, 20 μm.) (*G*) Surface plasmon resonance (SPR) measurements for S100A8, S100A9, or S100A8/S100A9 wt (2 μM) binding to immobilized PCNA. (*H*) SPR sensorgrams for S100A8/S100A9 N69A (0.06 to 1 μM) binding to PCNA measured using Biacore T200 ($\chi 2 = 8$). Kinetic data in Table 1.

recovered from the tissue of experimental mice. Even though T2AA did not fully normalize blood neutrophil counts, it significantly reduced pulmonary neutrophilia (Fig. 6*G*). Phenotypic profiling revealed that lung-infiltrating neutrophils display enhanced CXCR2 internalization and CD62L shedding in infected mice, characteristic of cell activation, and also showed increased percentage of immature-activated $CXCR2^{low}CD62L^{negative}$ subsets (Fig. 6*H*), as previously described in COVID-19 (42). Such effects were partially prevented by T2AA. Of note, T2AA treatment also significantly reduced both the frequency and protein expression of Arginase-1 in lung neutrophils, a marker reported in ongoing and convalescent COVID-19 patients (42). Furthermore, the proportion $CXCR2^{low}CD62L^{negative}Arg\text{-}1^{positive}$ neutrophils were markedly decreased in T2AA-treated mice (Fig. 6*I*). Together, these findings suggest that T2AA attenuates infection-induced pulmonary neutrophilia and limits the emergence of pathogenic and immature neutrophil subsets in the lung microenvironment.

Treatment increased circulating neutrophils but reduced lung neutrophil mediators, evidenced by decreased myeloperoxidase (MPO) activity and N-acetylglucosaminidase (NAG) (Fig. 6*J*). This coincided with reduced macrophage accumulation at the infection site, linked to lower C-X-C motif ligand 1 (CXCL1),

limiting neutrophil recruitment, and preserved transforming growth factor (TGF)-β (Fig. 6*K*), supporting immunoregulation. PCNA inhibitor reduced plasma S100A8/S100A9 and tended to lower lung levels (Fig. 6*L*), implicating PCNA–S100A8/S100A9 in COVID-19-related neutrophil lung injury. Lung but not plasma NET formation was markedly reduced (Fig. 6*M*). Immunostaining showed decreased MPO and neutrophil elastase (NE) in lung tissue, indicating reduced NET release. In situ detection revealed strong PCNA overexpression in lung neutrophils, underscoring its role in activation and NET generation (*SI Appendix*, Fig. S10). These in vivo data align with in vitro findings that T2AA blocks viral RNA–induced NET release. Overall, cytosolic PCNA is essential for neutrophil activation and NET formation in a COVID-like inflammation model, supporting its therapeutic targeting.

Discussion

Neutrophils are essential for infection control, but their timely clearance is crucial to resolving inflammation and preventing chronic conditions (43). The cytosolic PCNA scaffold is a highly dynamic protein complex that displays specific interactions in neutrophils depending on the inflammatory context (20, 44), for instance, associated with a strong interferon signature in neutrophils in COVID-19 (23). Here, we reveal that increased cytosolic PCNA associates with disease severity through a transcription-independent mechanism, extending observations from G-CSF–treated donors and other chronic inflammatory diseases (18). This event favors cell survival, potentially contributing to prolonged tissue damage in inflamed lungs (9, 12, 15, 45). Moreover, high intracellular PCNA was associated with NADPH oxidase-dependent ROS production and correlated with systemic neutrophil-derived markers predictive of severity, including NETs and calprotectin (7, 12, 25).

Unlike PCNA, both S100A8/S100A9 mRNA and S100A8 cytosolic levels were markedly upregulated in severe or critical COVID-19. Calprotectin, mainly localized in the neutrophil cytoplasm, is released with NETs (16) and promotes cell survival via TLR4–NF-κB signaling (46, 47). Despite elevated PCNA levels, calprotectin, accounting for ~40% of total cytosolic proteins (13), remains more abundant, indicating that only a fraction can interact with PCNA. We next provide mechanistic insights into the molecular and the functional characterization of PCNA-S100A8/S100A9 association. Calprotectin may assemble into different structures, forming heterodimers or heterotetramers depending on intracellular calcium concentrations. The S100A8/S100A9 heterocomplex activates TLR4/MD2, whereas calcium-induced tetramerization conceals the TLR4 site, restricting activation to local inflammation (31, 48). PCNA binds strongly to S100A8, but not S100A9 or the WT heterodimer, likely due to tetramer masking whereas a nontetramerizing mutant bound strongly, indicating tetramerization controls PCNA accessibility. In neutrophils, PCNA–S100A8/S100A9 association is promoted by NADPH oxidase activation and inhibited by T2AA. Besides, T2AA disrupted the PCNA–S100A8 interaction, an effect greatly reduced in HoxB8-S100A9 KO cells, indicating S100A8/S100A9 involvement in PCNA-dependent NADPH oxidase regulation. PCNA directly interacts with NADPH oxidase component $p47^{phox}$ (19) while S100A8 associates with $p67^{phox}$, Rac (32), and cytochrome b558 (33), suggesting that T2AA interferes with multiple associations between PCNA and NADPH-oxidase components. Given the complex PCNA interactome in COVID-19 neutrophils (23), T2AA likely also targets partners beyond S100A8, as previously reported (49).

Furthermore, we uncovered that PCNA-S100A8/S100A9 interaction was most pronounced in a subset of hyperactivated neutrophils, suggesting functional reprogramming in COVID-19 (4, 7, 8, 50). We confirmed neutrophil heterogeneity, including in LDN, identifying distinct subsets based on markers, such as CD66b, CD10, and LOX-1 expression, linked to early neutrophil development and thrombotic risk (4, 51, 52). Although LDN present a dysregulated immunophenotype (42, 51), we focused our analysis of the cytosolic PCNA scaffold on normal-density neutrophils, as we previously observed a pancellular distribution of PCNA in low-density subsets (20). In HD, PCNA-S100A8 interaction was mostly restricted to conventional $CD16^{high}/CD62L^{high}$ neutrophils. In severe COVID-19, it intensified and shifted to the $CD16^{high}/CD62L^{low}$ subset, characterized by high ROS production, CD11b, and LOX-1 expression, indicating a hyperactivated phenotype. This aligns with findings in LPS-challenged donors, where the $CD16^{high}/CD62L^{low}$ subset displays hypersegmented nuclei, increased activation markers, and NADPH-oxidase activity (36–38).

To assess the therapeutic potential of PCNA inhibition, we tested T2AA in a murine MHV-3–induced acute lung injury model mimicking severe COVID-19 with neutrophil-driven inflammation (39). Treatment significantly improved disease outcomes, likely by inducing cellular reprogramming and limiting recruitment rather than acting as an antiviral. T2AA did not lower circulating neutrophils, suggesting a shift toward proresolutive subsets instead of neutropenia. Interestingly, PCNA was minimally detected in epithelial cells but abundant in infiltrating neutrophils, colocalizing with MPO, underscoring its role in neutrophil-mediated lung inflammation. In vivo, T2AA reduced lung NET formation, consistent with human data showing inhibition of NETs induced by GM-CSF, C5a, or by viral RNA, a weak NADPH oxidase activator. Inhibition of PMA-induced NETs was observed only at early stages, suggesting a primary effect via NADPH oxidase suppression. These findings indicate that T2AA likely blocks NET formation through both NADPH oxidase–dependent and –independent mechanisms that remain to be elucidated. However, this effect on NET is not the only mechanism of action of T2AA, which acts on the control of several pathways including NADPH oxidase activation, glycolysis, and death pathways. Previously, T2AA reduced oxidative stress in murine colitis (19). Similarly, Paquinimod, which blocks extracellular S100A8/S100A9 via TLR4 inhibition, reversed neutrophil pathogenic phenotypes and lessened lung damage in SARS-CoV-2–infected mice and nonhuman primates, supporting both PCNA and calprotectin targeting in COVID-19 (53).

Our data provide mechanistic insights into the role of the PCNA scaffold in COVID-19–associated neutrophil hyperinflammation, highlighting the PCNA–S100A8/S100A9 interaction in activated subsets and the beneficial effects of disrupting the scaffold in vivo. Future studies unraveling the full spectrum of PCNA's molecular interactions will provide deeper insights into neutrophil dysfunction, paving the way for more innovative host-targeted therapies in inflammatory diseases.

Materials and Methods

Human Blood Samples. Individuals hospitalized due to COVID-19 from April 2020 to January 2022 were recruited in Paris, France from different departments of Cochin Hospital and Bichat Claude-Bernard Hospital. Patients were classified into different clinical severity groups (*SI Appendix*, Table S1) depending on a multifactorial score considering oxygen requirement (54). Blood from COVID-19 patients and HD obtained from the *Etablissement Français du Sang* was collected in EDTA or dry tubes for serum collection. Neutrophils were isolated in LPS-free dextran sedimentation and Ficoll (Histopaque-1077®, Sigma-Aldrich) centrifugation, as previously described (18).

Cell Lines. ER-Hoxb8 WT and S100A9 KO cells were cultured in OptiMEM Glutamax (Gibco, Thermo Fisher Scientific Waltham, MA) supplemented with 10% fetal bovine serum (FBS, Biowest, Nuaillé, France), 1% Pen/Strep (PAN-Biotech, Aidenbach, Germany), 30 μM ß-Mercaptoethanol (Sigma-Aldrich, St. Louis, MO), 1% stem cell factor supernatant (SCF, from SCF-producing CHO cells, Institute of Microbiology and Hygiene, Freiburg, Germany), and 1 μM ß-Estradiol (Sigma-Aldrich). For differentiation to mature neutrophils, cells were washed twice in PBS to remove ß-Estradiol and differentiated for 4 d in OptiMEM Glutamax supplemented with 10% FBS, 1% Pen/Strep, 30 μM ß-Mercaptoethanol (Sigma-Aldrich), and 1% SCF.

WT and gp91^{phox} KO PLB-985-derived cell lines were developed by Dinauer and colleagues (55) and differentiated with 0.5% *N*,*N*-dimethylformamide (DMF; Sigma) for 4 to 7 d in RPMI-1640 medium supplemented with 10 % (v/v) fetal calf serum, l-glutamine, and penicillin/streptomycin at 37 °C in 5 % CO_2.

Quantification of Circulating Neutrophil-Derived Activation Markers. Circulating neutrophil elastase (ThermoFisher Scientific), calprotectin (S100A8/S100A9) (Biotechne) and NETs were measured by ELISA as previously described (4).

Neutrophil Phenotype Assessment Using Spectral Flow Cytometry. Total blood or PBMC layer were labeled with the following antibodies: CD66b (G10F5), CD62L (DREG-56), CD16 (3G8), CD11b (ICRF44), CXCR2 (5E8), CD45 (2D1), PDL-1 (MH3), LOX-1 (15C4) from Biolegend; CD15 (W6D3), CD10 (HI10a), CD33 (P67.6), CD114 (LMM741), and PD-1 (EH12.1) from BD Biosciences; GLUT-1 (1418G) from R&D Systems or their respective isotypes. Samples were acquired (1000000 events) in a Cytek Aurora cytometer (Cytek Biosciences, Fremont, CA). Data were analyzed using FlowJo v10.7.1 software (FlowJo LLC) (*SI Appendix*, Figs. S6 and S7).

Assessment of Physiological Apoptosis. Neutrophils (2×10^5 cells/mL in RPMI-1640–10% FBS) were incubated overnight (16 h, 37 °C, 5% CO_2) and then labeled with annexin-V (Miltenyi Biotec) and 7-AAD (BD Biosciences) as previously described (18). To assess mitochondrial integrity, neutrophils were stained with 1 μM of 3,3′-dihexyloxacarbocyanine iodide (DiOC6) (ThermoFisher). Data acquisition was performed using BD-Accuri™-C6Plus, analyzed by Cflow Plus software.

Evaluation of NADPH-Oxidase-Dependent ROS Production. Neutrophils (0.1×10^6) were incubated in HBSS with or without T2AA (Sigma-Aldrich) for 1 h at 37 °C, then stimulated with PMA, opsonized zymosan, or fMLF (Sigma-Aldrich), as previously described (18). ROS production was measured by luminol-enhanced CL (TRISTAR luminometer, Bertold) and analyzed with microWim and Prism 9.3.

For subset analysis, neutrophils were stained with anti-CD16/CD62L after DCF-DA (5 μM, Thermo Fisher) loading and analyzed by flow cytometry.

In a separate assay, cells (3×10^5) were preincubated with 1 μM T2AA for 1 h, stimulated with 10 nM PMA for 15 min, washed, and incubated with 15 μM DHR123 (Sigma-Aldrich) for 15 min. Samples were analyzed by flow cytometry (CytoFlex S, Beckman Coulter) using FlowJo v10.10.0 (BD Life Sciences, Ashland, OR).

Evaluation of NET Formation. Neutrophils (2.5×10^6/mL) were seeded on 12-mm glass coverslips in X-VIVO 15 medium (Lonza), primed with GM-CSF (25 ng/mL), and stimulated with C5a (10 nM) or PMA (25 nM) for up to 2 h. Cells were preincubated or not with inhibitors (T2AA, 10 μM; DPI, 10 μM) for 30 min at 37 °C before stimulation. For extracellular DNA detection, MitoSOX Red (5 μM) was added for the last 15 min, followed by fixation (4% PFA) and Hoechst 33342 staining. Imaging was performed on an LSM 800 (Zeiss) and analyzed with IMARIS, as previously reported (56). For DNA quantification in supernatants, DNase I (2.5 U/mL) (Worthington) was added. The reaction stopped with EDTA (Sigma-Aldrich) and mixed with PicoGreen dye (Invitrogen). Fluorescence was measured at 502/523 nm using a SpectraMax M2 spectrofluorometer (Molecular Devices).

Also for NET visualization, neutrophils (5×10^6/mL) on polylysine-coated slides were pretreated with T2AA or CU-CPT9a (NET inhibition control) for 30 min, then stimulated with SARS-CoV mRNA (10 μg/mL, DOTAP) for 1 h. Cells were fixed (1% PFA), stained with anti-citrullinated histone H4 and Alexa-488 secondary antibody (Ab81797, Abcam), followed by an Alexa-488 conjugated anti-rabbit antibody (Thermo Fisher Scientific) and counterstained with Hoechst, and imaged on a Zeiss Observer.Z1 with Apotome2. NET production was also quantified by DNA-associated elastase activity. Neutrophils (2.5×10^6/mL) in 96-well plates were treated as above, digested with DNase I (1 U/mL), and elastase activity measured with 0.5 mM of the fluorogenic substrate (Z-Ala-Ala-Ala-Ala) AMC (Cayman Chemical) using a fluorescence plate reader.

Western Blot Analysis of PCNA and S100A8. Neutrophil cytosol was obtained by sonication in hypotonic HEPES buffer (50 mM) supplemented with protease and phosphatase inhibitors (4 mM PMSF, 400 μM leupeptin, 400 μM pepstatin, 1 mM orthovanadate, 1 mM EGTA, 1 mM EDTA) and 1 mM DTT, using a Soniprep 150 Plus (1 Hz, 10 s). Protein concentration was measured using the BCA kit (Pierce). Cytosolic proteins (30 μg) diluted in Laemmli buffer were separated by SDS-PAGE and transferred to PVDF membranes (PerkinElmer). After blocking in 5% nonfat dry milk in TBS, membranes were incubated overnight at 4 °C with mouse anti-PCNA (PC10; 1:1,000), goat anti-S100A8 (Everest, EB11513; 1:1,000), or goat anti-actin (Sigma A2066; 1:1,000). HRP-conjugated secondary antibodies (anti-rabbit IgG, 1:5000; anti-mouse IgG, 1:2,000; anti-goat IgG, 1:4,000) were applied for 1 h at room temperature (18). Immunoreactive bands were visualized using ECL (Amersham) and quantified with the Fusion FX7 imaging system (Vilbert Lourmat).

PCNA, S100A8, and S100A8/S100A9 Detection Using Indirect Immunofluorescence or the Duolink® PLA. Cells were fixed in 2% formaldehyde/PBS (20 min, on ice), permeabilized with 0.25% Triton X-100 (5 min, RT), and treated with ice-cold methanol (10 min). For immunofluorescence, cells were incubated with anti-PCNA (Ab5; 1:25) or anti-S100A8 (2H2; 1:100) for 45 min, followed by biotinylated anti-rabbit IgG (1:200) and streptavidin-Alexa Fluor 555 (1:1,000) for PCNA, or anti-mouse IgG Alexa Fluor 488 (1:100) for S100A8. Nuclei were counterstained with DAPI mounting medium.

For Duolink® PLA, neutrophils (0.3×10^6) were processed according to the manufacturer's protocol using anti-PCNA (Ab5; 1:100) with anti-S100A8 (2H2; 1:100) or anti-S100A9 (2B10; 1:100) on cytospins or in suspension. PLA signal was generated when epitopes were ≤40 nm apart. Microscopy was performed using Widefield Zeiss Observer Z1, IXplore spinning confocal, or Leica SP8X STED FLIM, and at least 30 cells/group were analyzed with FIJI software (v2.14.0/1.54j). For flow cytometry PLA, ≥100,000 events were acquired on a Cytek Aurora.

Analysis of PCNA-S100A8 Interaction by SPR. Interactions between PCNA and recombinant human (rh) S100 proteins (R&D Systems, Biotechne, MN) and recombinant mutant human S100 proteins (provided by Thomas Vogl's laboratory) were analyzed by SPR using a Biacore T200 (GE Healthcare) to determine affinity and kinetic parameters (19). PCNA was immobilized on a dextran sensor chip (CM5), while rhS100A8 (9876-S8), S100A9 (9254-S9), S100A8/S100A9 complex (8226-S8), or) and rh S100A8/S100A9 N69A mutant (0.1 to 2 μM) were used as analytes in running buffer (HEPES 20 mM, NaCl 140 mM, CaCl2 0.5 mM, ZnCl2 10 μM, pH 7.4). Specific binding signals were obtained by subtracting background signals. Kinetic titration (multiple-cycle kinetics) was performed with sequential analyte injections over the immobilized ligand, with 5 mM EDTA used for regeneration. Association (Ka) and dissociation (Kd) rate constants and KD values were calculated using BIAevaluation software. A 1:1 Langmuir model was tested first, but also the heterogeneous ligand model, accounting for two independent binding sites.

In Vivo Experiments. Experiments were carried out with male and female C57BL/6 mice aged of 6 to 7 wk from the Central Animal House from Universidade Federal de Minas Gerais (UFMG). Mice were housed in individually ventilated cages placed in an animal care facility at 24 °C ± 2 °C on a 12-h light/12 h dark cycle, receiving ad libitum access to water and food. Animal welfare and experimental procedures were carried out strictly in accordance with the Guide for the Care and Use of Laboratory Animals (NIH) and followed the ARRIVE guidelines.

Mouse Hepatitis Virus Strain 3-Induced Acute Lung Injury. Mice were intranasally inoculated with MHV-3 (3×10^3 PFU), a coronavirus strain that recapitulates key features of severe COVID-19, including neutrophil-driven lung inflammation (39), and treated with T2AA (0.5 mg/kg, i.p.) starting 24 h postinfection. Lung pathology was evaluated on Day 3 (peak infection) via histological scoring (Hemalun eosin staining), viral load quantification (plaque assay), and cytokine/chemokine profiling (ELISA for TGF-beta and CXCL-1/2). Neutrophil activation was assessed using flow cytometry ($Ly6G^+CXCR2^+CD62L^+$ cells),

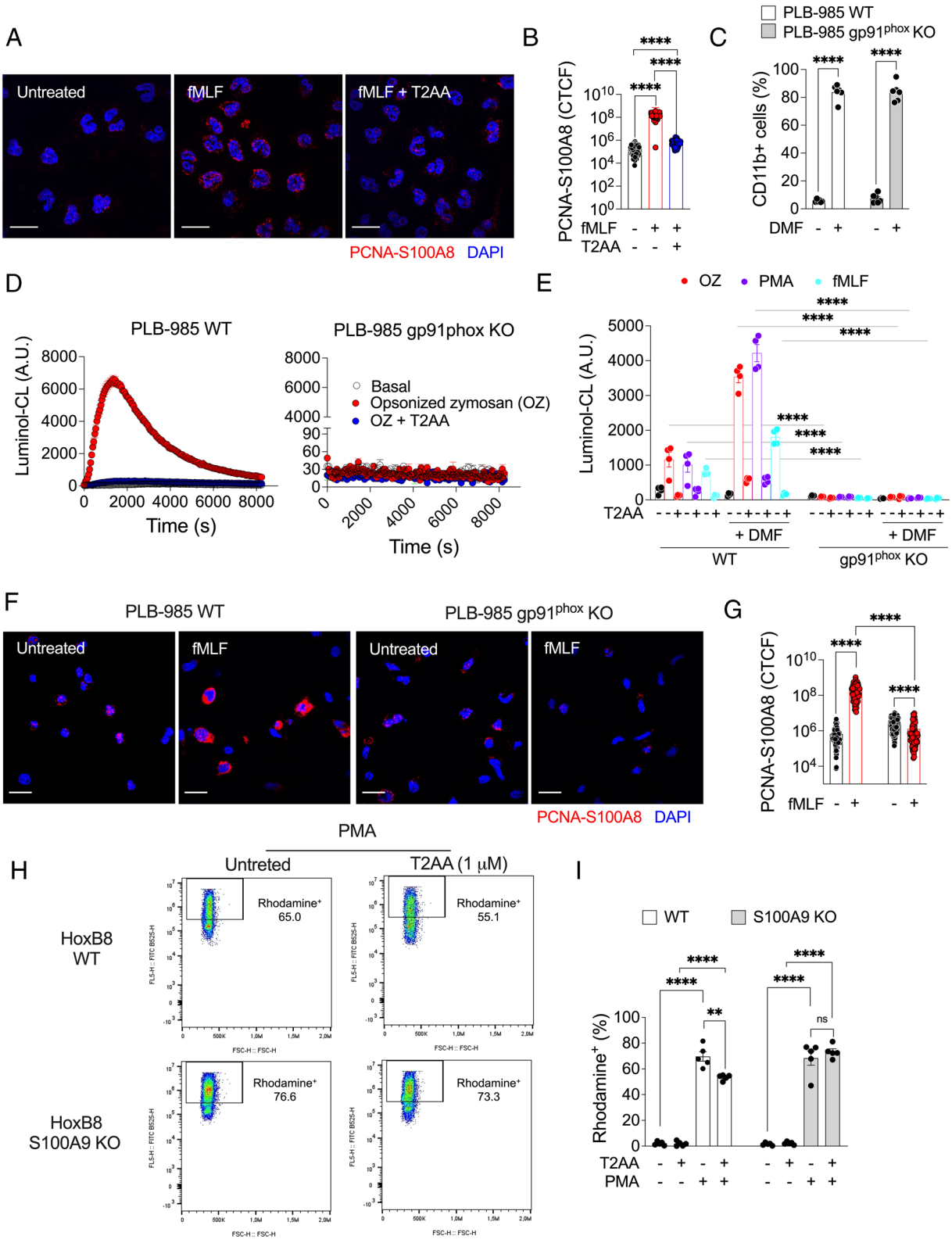

Fig. 4. Modulation of PCNA-S100A8 interaction by NADPH-oxidase activation. (*A* and *B*) Duolink® PLA detecting PCNA–S100A8 interaction (red) in human neutrophils. Blue fluorescence indicates nuclei. Effect of T2AA (10 μM) with fMLF (1 μM) on PCNA–S100A8 interaction was tested. (*B*) PCNA–S100A8 signal as CTCF for three independent healthy donors' neutrophils (n = 90 cells/group). Mean ± SEM; analyzed by Kruskal–Wallis followed by Dunn's test (****$P < 0.0001$). (Scale bar, 20 μm.) (*C–E*) Wild-type (WT) and GP91phox-knockout (KO) PLB-985 neutrophil-like cells. (*C*) Percentage of CD11b-positive cells in undifferentiated and DMF-differentiated PLB-985 cells (n = 6 biological replicates). Mean ± SEM; analyzed by the unpaired *t* test (****$P < 0.0001$). (*D* and *E*) Cells stimulated with opsonized zymosan (OZ, 0.5 mg/mL), PMA (0.1 μg/mL), or fMLF (1 μM) with or without T2AA (10 μM). NADPH oxidase–dependent ROS production measured by luminol-enhanced CL over time. (*D*) Representative kinetic curves with OZ. (*E*) Peak ROS values for all stimuli in WT and KO cells (n = 4 biological replicates). Mean ± SEM; analyzed by the unpaired *t* test (undifferentiated vs DMF-differentiated or WT vs KO, ****$P < 0.0001$). (*F* and *G*) PLA for PCNA–S100A8 interaction in differentiated PLB-985 cells stimulated or not with fMLF. (*F*) Representative experiment from three independent biological replicates. (*G*) Quantification of PLA signal (CTCF) for n = 95 cells/group. Mean ± SEM; analyzed by Mann–Whitney test (****$P < 0.0001$). (Scale bar, 15 μm.) (*H* and *I*) NADPH-dependent ROS production in WT and S100A9-KO HoxB8 cells. ROS was measured by flow cytometry as percentage of rhodamine-positive cells after incubation with or without PMA (10 nM, 15 min) or T2AA (1 μM). (*H*) Representative dot plots from PMA-stimulated groups with gates set above basal ROS levels. (*I*) Data from five independent experiments. Mean ± SEM; analyzed by the paired *t* test (**$P < 0.01$, ****$P < 0.0001$, ns = not significant).

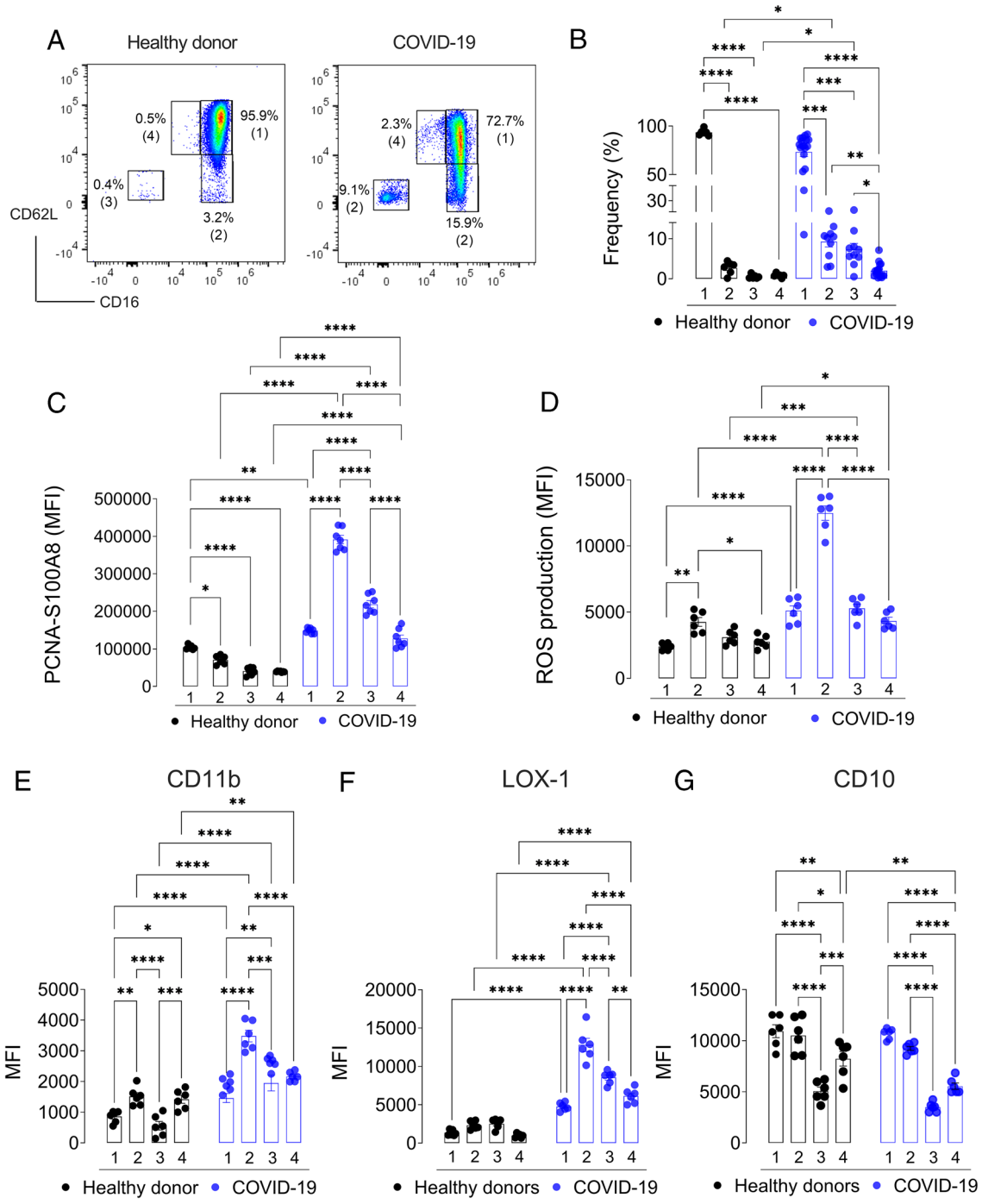

Fig. 5. PCNA-S100A8 interaction is increased in a hyperactivated neutrophil subset in COVID-19. (*A*) Representative flow cytometry dot plot of neutrophil subsets defined by CD16/CD62L expression. (*B*) Distribution (%) of subsets: CD16high/CD62Lhigh (1), CD16high/CD62Llow (2), CD16low/CD62Llow (3), and CD16low/CD62Lhigh (4) in HD (n = 6) and COVID-19 patients (n = 18, 10, 10, and 18, respectively). (*C*) Duolink® PLA quantification of PCNA–S100A8 interactions across subsets (n = 6 per group). (*D*) ROS production measured by 5 μM DCF-DA labeling (n = 6 per group). (*E–G*) Surface expression of CD11b (*E*), LOX-1 (*F*), and CD10 (*G*) in neutrophil subsets (n = 6 per group). (*B–G*) Mean ± SEM; analyzed by one-way ANOVA followed by the Tukey post test (**P* < 0.05, ***P* < 0.01, ****P* < 0.001, *****P* < 0.0001).

MPO/NAG enzymatic assays, NETs and S100A8/A9/MPO-DNA complexes. Full methodological details, including sample preparation, staining, and analytical pipelines, are available in *SI Appendix*, Supporting Methods.

Statistics. Data are expressed as mean ± SEM from independent experiments (n, as indicated in each figure). Data distribution was assessed using the Kolmogorov–Smirnov and Shapiro–Wilk normality tests. For normally distributed data, one-way ANOVA followed by the Tukey post hoc test was applied for multiple comparisons and paired or unpaired Student's *t* test was used for two-group comparisons. For nonparametric data, the Kruskal–Walli's test followed by Dunn's post hoc test was applied for multiple comparisons, and the Mann–Whitney test was used for two-group comparisons. Data were analyzed using GraphPad Prism Software 9.0, and $P < 0.05$ was considered statistically significant.

Study Approval. Ethical approval for human investigations was granted by the Institutional Review Board and Ethics Committee of Cochin Hospital, Paris, France (Internal Medicine Department: authorization #2019-3677; Pneumology Department: authorization #2020 #A02700-39; Intensive Care Department: authorization #2018 #A01934-51) and by the Ethics Committee of Bichat Hospital, Paris, France (Intensive Care Department: authorization #2020-715)

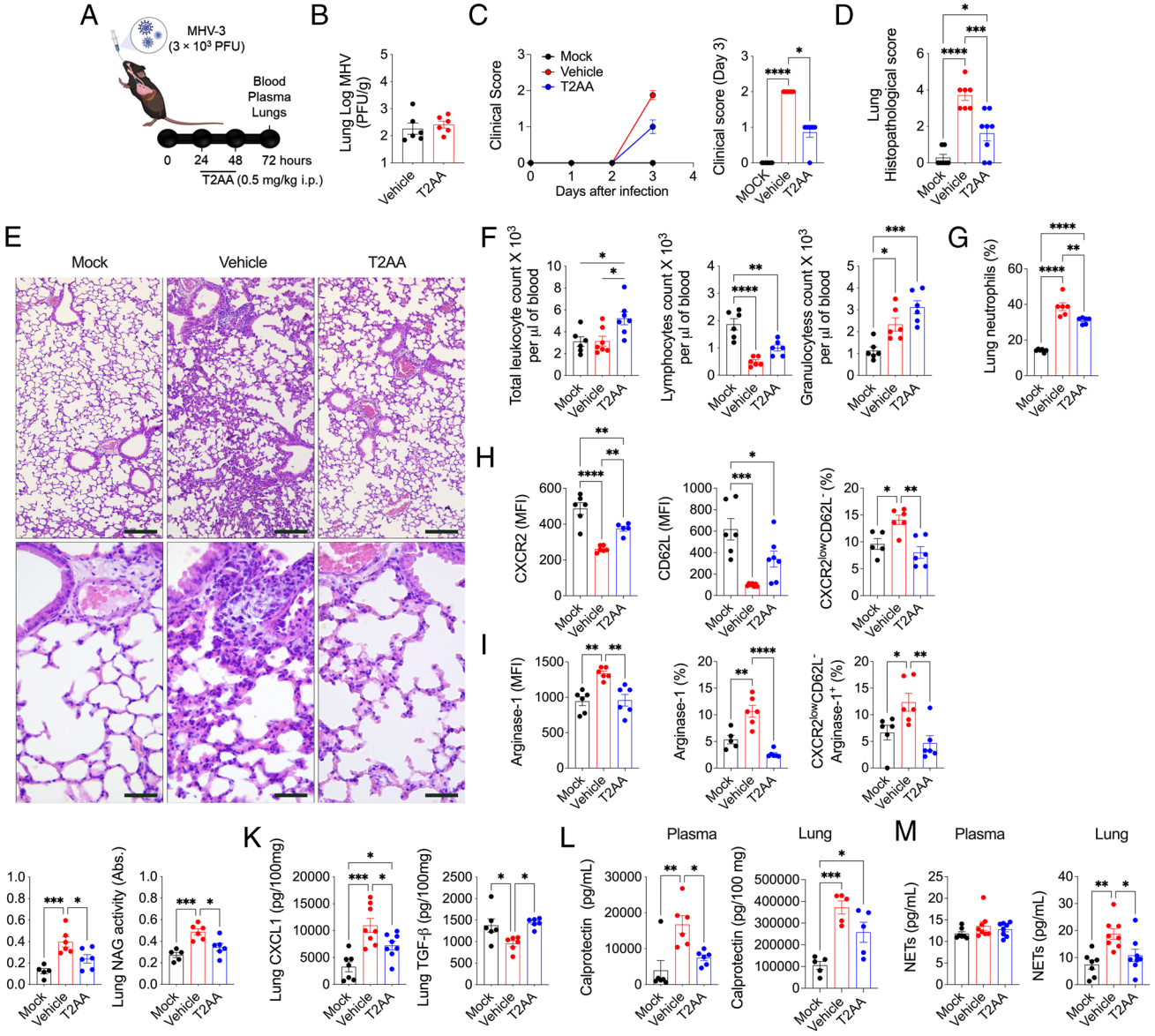

Fig. 6. PCNA inhibition by T2AA reduces lung damage in betacoronavirus MHV-3-infected mice affecting neutrophils-driven inflammation. (*A*) C57BL/6 mice infected with MHV-3 (3 × 10^3 PFU) or mock-treated, then given T2AA (0.5 mg/kg, i.p.) or vehicle every 12 h. Blood and lungs were collected after 3 d. (*B*) Viral load (log_{10} PFU/g) in lungs (n = 6). Mean ± SEM; analyzed by the unpaired *t* test ($P > 0.05$). (*C*) Clinical scores based on death, weight, symptoms, and behavior (n = 6 to 8). (*E*) Histopathological scoring of lungs (n = 7 to 8). (*C* and *D*) Mean ± SEM; analyzed by Kruskal–Wallis test followed by Dunn's post test (*$P < 0.05$, ***$P < 0.001$, ****$P < 0.0001$). (*E*) Representative lung histology (H&E, 40×). (Scale bar, 50 µm.) (*F*) Blood cell counts (×10^3/µL) (n = 6 to 7). (*G–I*) Flow cytometry of viable neutrophils ($CD45^+Ly6G^+F4/80^-$) from lung tissue (n = 5 to 6). Percentages and membrane levels of CXCR2, CD62L, and Arginase-1 are shown. (*J*) Neutrophil and macrophage infiltration measured by MPO and NAG activity (mOD/mg tissue) in lung tissue (n = 5 to 6). (*K*) CXCL1 and TGF-β levels (pg/100 mg lung, n = 6 to 8). (*L* and *M*) S100A8/S100A9 and NETs quantification in plasma (pg/mL) and lungs homogenates (pg/100 mg tissue) (n = 5 to 8). (*F–M*) Mean ± SEM; analyzed by one-way ANOVA followed by the Tukey post test (*$P < 0.05$, **$P < 0.01$, ***$P < 0.001$, ****$P < 0.001$).

in accordance with the Declaration of Helsinki. Written informed consent was obtained from all hospitalized participants prior to enrollment. All experimental procedures involving mice were approved by the Ethical Committee for Animal Experimentation of the Federal University of Minas Gerais (UFMG), Brazil (protocol #190/2020).

Data, Materials, and Software Availability. All study data are included in the article and/or *SI Appendix*.

ACKNOWLEDGMENTS. We thank Léa Rémy-Tourneur for Western blot analysis, technical support to Lucie Pesenti, and drafting the initial manuscript and to Mary Dinauer who provided PLB-985 cells and gave manuscript feedback. Thanks to Thomas Guilbert (IMAGIC/Institut Cochin), Molly Ingersoll, and Karen Aymonnier for their input. This work was funded by the Fondation pour la Recherche Médicale (EQU202003010155, V.W.-S.), ANR programs (IDEX-0005-02, LabEx INFLAMEX, V.W.-S.; LABX-62 IBEID, A.H.; RA-COVID-19 V5-COVINNATE, M.H.-N.; DENDRISEPSIS and APCOD, F.P.), and FAPESP-SCRIPPS (15/50387-4, F.S.). H.-U.S. was supported by the Swiss NSF (310030_184816). Additional support came from INCT Dengue CNPq (465425/2014-3), FAPEMIG (25036/2014-3; RED-00202-22; APQ-02281-18; APQ-02618-23), CAPES (88881.507175/2020-01), and Deutsche Forschungsgemeinschaft (CRC1450 C3, TRR332 C7, CRU342 P5, T.V.). Rodrigo Formiga was funded by Campus France (Le programme de bourses France Excellence Eiffel) and CAPES/PRINT (PhD fellowship); Lucie Pesenti by LabEx INFLAMEX (PhD fellowship); François Chable de la Héronnière by Vaincre la Mucoviscidose (PhD fellowship).

Author affiliations: [a]Université Paris Cité, CNRS UMR 8104, Inserm U1016, Paris 75014, France; [b]Institut Cochin, Paris 75014, France; [c]Department of Pharmacology, Federal University of Santa Catarina, Florianópolis, Santa Catarina 88040-900, Brazil; [d]Institute of Pharmacology, University of Bern, Bern 3010, Switzerland; [e]Université Grenoble Alpes, CNRS, Institute of Structural Biology (IBS) - UMR 5075, Grenoble 38044, France; [f]Institute of Immunology, University of Münster, Münster 48149, Germany; [g]Department of Molecular and Translational Medicine, University of Brescia, Brescia 25123, Italy; [h]Laboratory of Systems Biology, Department of Microbiology, Immunology and Parasitology, Federal University of Santa Catarina, Florianópolis, Santa Catarina 88040-900, Brazil; [i]Bioinformatics Core Platform, INSERM Unit 1163, Imagine Institute, Université Paris Cité, Paris 75015, France; [j]Center for Research in Inflammatory Diseases, Ribeirão Preto Medical School, University of São Paulo, Ribeirão Preto, São Paulo 14049-900, Brazil; [k]Department of Morphology, Institute of Biological Sciences, Federal University of Minas Gerais, Belo Horizonte, Minas Gerais 31270-901, Brazil; [l]Department of Microbiology, Institute of Biological Sciences, Federal University of Minas Gerais, Belo Horizonte, Minas Gerais 31270-901, Brazil; [m]Department of Biochemistry and Immunology, Institute of Biological Sciences, Federal University of Minas Gerais, Belo Horizonte, Minas Gerais 31270-901, Brazil; [n]Assistance Publique–Hôpitaux de Paris (AP-HP), Department of Immunology, Bichat Hospital, Paris 75018, France; [o]Université Paris cité, INSERM UMR 1149, Paris, France; [p]Department of Internal Medicine, Assistance Publique–Hôpitaux de Paris (AP-HP), Cochin Hospital, Paris 75014, France; [q]Department of Immunology and Hematology, Functional Unit of Immune Dysfunctions, Hôpitaux Universitaires Paris Nord Val-de-Seine, Bichat Hospital, Paris 75018, France; [r]Department of Respiratory Medicine, Assistance Publique–Hôpitaux de Paris (AP-HP), Cochin Hospital, Paris 75014, France; [s]Institute of Biochemistry, Brandenburg Medical School, Neuruppin 16816, Germany; [t]Department of Medicine, Section of General Pathology, University of Verona, Verona 37134, Italy; and [u]Department of Intensive Medicine and Reanimation, Assistance Publique–Hôpitaux de Paris (AP-HP), Cochin Hospital, Paris 75014, France

Author contributions: R.d.O.F., A.H., M.A.C., V.V.C., and V.W.-S. designed research; R.d.O.F., L.P., F.C.d.l.H., M.Z.L., D.S., S.Y., P.F., L.K., L.T., D.B., M.A., S.M., V.K., K.B., G.S.-T., M.C., C.R., C.J.L.d.R.A., A.d.S.R., F.Q.C., J.C.A.-F., N.R.C.N., M.R.G., C.M.Q.-J., V.L.B., M.M.T., V.G., S.C.-M., L.D.C., L.M., M.H.-N., C.M., F.S., H.-U.S., N.T., M.A.C., F.P., T.V., P.-R.B., V.V.C., and V.W.-S. performed research; L.P., S.Y., M.A., F.Q.C., J.C.A.-F., M.M.T., S.C.-M., L.M., A.H., M.H.-N., C.M., F.S., H.-U.S., F.P., T.V., P.-R.B., V.V.C., and V.W.-S. contributed new reagents/analytic tools; R.d.O.F., L.P., F.C.d.l.H., M.Z.L., D.S., S.Y., P.F., L.K., L.T., D.B., S.M., V.K., K.B., T.D., C.R., M.R.S., E.L.d.R., E.P.L., M.R.G., C.M.Q.-J., V.L.B., C.M., H.-U.S., N.T., M.A.C., F.P., T.V., P.-R.B., V.V.C., and V.W.-S. analyzed data; and R.d.O.F. and V.W.-S. wrote the paper.

The authors declare no competing interest.

1. W. M. Nauseef, The phagocyte NOX2 NADPH oxidase in microbial killing and cell signaling. *Curr. Opin. Immunol.* **60**, 130–140 (2019).
2. M. Lourda *et al.*, High-dimensional profiling reveals phenotypic heterogeneity and disease-specific alterations of granulocytes in COVID-19. *Proc. Natl. Acad. Sci. U.S.A.* **118**, e2109123118 (2021).
3. J. Schulte-Schrepping *et al.*, Severe COVID-19 is marked by a dysregulated myeloid cell compartment. *Cell* **182**, 1419–1440.e23 (2020).
4. M. Peyneau *et al.*, Innate immune deficiencies are associated with severity and poor prognosis in patients with COVID-19. *Sci. Rep.* **12**, 638 (2022).
5. R. de Oliveira Formiga *et al.*, Neuraminidase is a host-directed approach to regulate neutrophil responses in sepsis and COVID-19. *Br. J. Pharmacol.* **180**, 1460–1481 (2023).
6. C. Huang *et al.*, Clinical features of patients infected with 2019 novel coronavirus in Wuhan. *China. Lancet* **395**, 497–506 (2020).
7. A. Silvin *et al.*, Elevated calprotectin and abnormal myeloid cell subsets discriminate severe from mild COVID-19. *Cell* **182**, 1401–1418.e18 (2020).
8. J. T. deKay *et al.*, DespRhigh neutrophils are associated with critical illness in COVID-19. *Sci. Rep.* **11**, 22463 (2021).
9. L. Reyes *et al.*, A type I IFN, prothrombotic hyperinflammatory neutrophil signature is distinct for COVID-19 ARDS. *Wellcome Open Res.* **6**, 38 (2021).
10. Q.-X. Long *et al.*, Clinical and immunological assessment of asymptomatic SARS-CoV-2 infections. *Nat. Med.* **26**, 1200–1204 (2020).
11. S. Li *et al.*, Clinical and pathological investigation of patients with severe COVID-19. *JCI Insight* **5**, 138070 (2020).
12. F. P. Veras *et al.*, SARS-CoV-2-triggered neutrophil extracellular traps mediate COVID-19 pathology. *J. Exp. Med.* **217**, e20201129 (2020).
13. M. Pruenster, T. Vogl, J. Roth, M. Sperandio, S100A8/S100A9: From basic science to clinical application. *Pharmacol. Ther.* **167**, 120–131 (2016).
14. V. Brinkmann *et al.*, Neutrophil extracellular traps kill bacteria. *Science* **303**, 1532–1535 (2004).
15. A. Hosseini *et al.*, Transcriptional insights of oxidative stress and extracellular traps in lung tissues of fatal COVID-19 cases. *Int. J. Mol. Sci.* **24**, 2646 (2023).
16. E. G. G. Sprenkeler *et al.*, S100A8/S100A9 is a marker for the release of neutrophil extracellular traps and induces neutrophil activation. *Cells* **11**, 236 (2022).
17. E. Gardiman *et al.*, SARS-CoV-2-associated ssRNAs activate human neutrophils in a TLR8-dependent fashion. *Cells* **11**, 3785 (2022).
18. V. Witko-Sarsat *et al.*, Proliferating cell nuclear antigen acts as a cytoplasmic platform controlling human neutrophil survival. *J. Exp. Med.* **207**, 2631–2645 (2010).
19. D. Ohayon *et al.*, Cytosolic PCNA interacts with p47phox and controls NADPH oxidase NOX2 activation in neutrophils. *J. Exp. Med.* **216**, 2669–2687 (2019).
20. K. Aymonnier *et al.*, G-CSF reshapes the cytosolic PCNA scaffold and modulates glycolysis in neutrophils. *J. Leukoc. Biol.* **115**, 205–221 (2024).
21. Z. Kelman, PCNA: Structure, functions and interactions. *Oncogene* **14**, 629–640 (1997).
22. D. Bouayad *et al.*, Nuclear-to-cytoplasmic relocalization of the proliferating cell nuclear antigen (PCNA) during differentiation involves a chromosome region maintenance 1 (CRM1)-dependent export and is a prerequisite for PCNA antiapoptotic activity in mature neutrophils. *J. Biol. Chem.* **287**, 33812–33825 (2012).
23. L. Pesenti *et al.*, Neutrophils display novel partners of cytosolic proliferating cell nuclear antigen involved in interferon response in COVID-19 patients. *J. Innate Immun.* **17**, 154–175 (2025).
24. A. Inoue *et al.*, A small molecule inhibitor of monoubiquitinated Proliferating Cell Nuclear Antigen (PCNA) inhibits repair of interstrand DNA cross-link, enhances DNA double strand break, and sensitizes cancer cells to cisplatin. *J. Biol. Chem.* **289**, 7109–7120 (2014).
25. R. L. Chua *et al.*, COVID-19 severity correlates with airway epithelium–immune cell interactions identified by single-cell analysis. *Nat. Biotechnol.* **38**, 970–979 (2020).
26. J. Carvelli *et al.*, Association of COVID-19 inflammation with activation of the C5a–C5aR1 axis. *Nature* **588**, 146–150 (2020).
27. B. M. Silva *et al.*, C5aR1 signaling triggers lung immunopathology in COVID-19 through neutrophil extracellular traps. *J. Clin. Invest.* **133**, e163105 (2023).
28. S. Yousefi *et al.*, Untangling "NETosis" from NETs. *Eur. J. Immunol.* **49**, 221–227 (2019).
29. E. F. Kenny *et al.*, Diverse stimuli engage different neutrophil extracellular trap pathways. *eLife* **6**, e24437 (2017).
30. A. Buck *et al.*, DPI selectively inhibits intracellular NADPH oxidase activity in human neutrophils. *Immunohorizons* **3**, 488–497 (2019).
31. N. Leukert *et al.*, Calcium-dependent tetramer formation of S100A8 and S100A9 is essential for biological activity. *J. Mol. Biol.* **359**, 961–972 (2006).
32. C. Kerkhoff *et al.*, The arachidonic acid-binding protein S100A8/S100A9 promotes NADPH oxidase activation by interaction with p67phox and Rac-2. *FASEB J.* **19**, 467–469 (2005).
33. S. Berthier *et al.*, Molecular interface of S100A8 with cytochrome b558 and NADPH oxidase activation. *PLoS One* **7**, e40277 (2012).
34. L.-A.H. Allen, Closing the gap between murine neutrophils and neutrophil-like cell lines. *J. Leukoc. Biol.* **114**, 199–201 (2023).
35. M.-P. Manitz *et al.*, Loss of S100A9 (MRP14) results in reduced interleukin-8-induced CD11b surface expression, a polarized microfilament system, and diminished responsiveness to chemoattractants in vitro. *Mol. Cell Biol.* **23**, 1034–1043 (2003).
36. J. Pillay *et al.*, A subset of neutrophils in human systemic inflammation inhibits T cell responses through Mac-1. *J. Clin. Invest.* **122**, 327–336 (2012).
37. R. Spijkerman *et al.*, Flow cytometric evaluation of the neutrophil compartment in COVID-19 at hospital presentation: A normal response to an abnormal situation. *J. Leukoc. Biol.* **109**, 99–114 (2021).
38. R. Spijkerman *et al.*, An increase in CD62Ldim neutrophils precedes the development of pulmonary embolisms in COVID-19 patients. *Scand. J. Immunol.* **93**, e13023 (2021).
39. A. C. D. S. P. Andrade *et al.*, A biosafety level 2 mouse model for studying betacoronavirus-induced acute lung damage and systemic manifestations. *J. Virol.* **95**, e0127621 (2021).
40. T. M. L. Souza *et al.*, Preclinical development of kinetin as a safe error-prone SARS-CoV-2 antiviral able to attenuate virus-induced inflammation. *Nat. Commun.* **14**, 199 (2023).
41. R. das D. Pereira *et al.*, A 5-lipoxygenase inhibitor, zileuton, modulates host immune responses and improves lung function in a model of severe acute respiratory syndrome (SARS) induced by betacoronavirus. *Viruses* **15**, 2049 (2023).
42. A. Dwivedi *et al.*, Emergence of dysfunctional neutrophils with a defect in arginase-1 release in severe COVID-19. *JCI Insight* **9**, e171659 (2024).
43. K. R. Martin, D. Ohayon, V. Witko-Sarsat, Promoting apoptosis of neutrophils and phagocytosis by macrophages: Novel strategies in the resolution of inflammation. *Swiss Med. Wkly.* **145**, w14056 (2015).
44. L.-A.H. Allen, PCNA at the crossroads of human neutrophil activation, metabolism, and survival. *J. Leukoc. Biol.* **115**, 201–204 (2024).
45. C. Radermecker *et al.*, Neutrophil extracellular traps infiltrate the lung airway, interstitial, and vascular compartments in severe COVID-19. *J. Exp. Med.* **217**, e20201012 (2020).
46. D. Chakraborty *et al.*, Alarmin S100A8 activates alveolar epithelial cells in the context of acute lung injury in a TLR4-dependent manner. *Front. Immunol.* **8**, 1493 (2017).
47. D. H. Kim *et al.*, Suppressive effects of S100A8 and S100A9 on neutrophil apoptosis by cytokine release of human bronchial epithelial cells in asthma. *Int. J. Med. Sci.* **17**, 498–509 (2020).
48. T. Vogl *et al.*, Autoinhibitory regulation of S100A8/S100A9 alarmin activity locally restricts sterile inflammation. *J. Clin. Invest.* **128**, 1852–1866 (2018).
49. C. Olaisen, R. Müller, A. Nedal, M. Otterlei, PCNA-interacting peptides reduce Akt phosphorylation and TLR-mediated cytokine secretion suggesting a role of PCNA in cellular signaling. *Cell. Signal.* **27**, 1478–1487 (2015).
50. H. Shi *et al.*, Neutrophil calprotectin identifies severe pulmonary disease in COVID-19. *J. Leukoc. Biol.* **109**, 67–72 (2021).
51. B. Combadière *et al.*, LOX-1–expressing immature neutrophils identify critically-ill COVID-19 patients at risk of thrombotic complications. *Front. Immunol.* **12**, 752612 (2021).
52. K. Mukund *et al.*, Immune response in severe and non-severe Coronavirus disease 2019 (COVID-19) infection: A mechanistic landscape. *Front. Immunol.* **12**, 738073 (2021).
53. Q. Guo *et al.*, Induction of alarmin S100A8/S100A9 mediates activation of aberrant neutrophils in the pathogenesis of COVID-19. *Cell Host Microbe* **29**, 222–235.e4 (2021).
54. R. Mellado-Artigas *et al.*, High-flow nasal oxygen in patients with COVID-19-associated acute respiratory failure. *Crit. Care* **25**, 58 (2021).
55. L. Zhen *et al.*, Gene targeting of X chromosome-linked chronic granulomatous disease locus in a human myeloid leukemia cell line and rescue by expression of recombinant gp91phox. *Proc. Natl. Acad. Sci.* **90**, 9832–9836 (1993).
56. D. Stojkov *et al.*, ROS and glutathionylation balance cytoskeletal dynamics in neutrophil extracellular trap formation. *J. Cell Biol.* **216**, 4073–4090 (2017).